Scanning Probe Lithography. 4. Characterization of Scanning Tunneling Microscope-Induced Patterns in *n*-Alkanethiol Self-Assembled Monolayers

Jonathan K. Schoer and Richard M. Crooks*

Department of Chemistry, Texas A&M University, College Station, Texas 77845-3255

Received April 16, 1996. In Final Form: February 6, 1997[⊗]

Self-assembled monolayers (SAMs) of *n*-alkanethiol molecules adsorbed onto Au(111) substrates act as lithographic resists, which can be selectively patterned using scanning tunneling microscopy (STM). We previously provided evidence that patterning is the result of faradaic electrochemical processes. Here, we provide a more detailed model for the patterning mechanism that involves penetration of the tip into the SAM, concerted SAM disruption, and subsequent SAM removal arising from electrochemical processes. Experiments, and a detailed analysis of the patterned features, are consistent with this model. Other key results of this study include the following: (1) the electrochemical nature of the patterning process defines the resolution of STM patterning under the conditions used in this study; (2) lithographically defined patterns are dimensionally stable for several days; (3) the STM tip penetrates the monolayer and very slowly modifies it regardless of bias and tunneling current.

Introduction

In a previous paper we provided evidence that scanning tunneling microscope (STM)-induced patterning of organomercaptan self-assembled monolayers (SAMs) in air and N_2 at biases between ∼+2.3 and ∼+3.0 V arises from a faradaic electrochemical process.[1] Here we expand on those results and provide supporting evidence for an electrochemical process as well as a detailed description of the patterns.

Organomercaptans adsorb onto some metal[2−8] and semiconductor[9−12] surfaces to yield ultrahigh density monolayers up to 3 nm thick. These monolayers can be viewed as resists for STM lithography since they effectively passivate surfaces against many mass- and electron-transfer processes,[4,13−26] but do not prevent electron tunneling from STM tips. Organomercaptan SAM resists have previously been patterned by a variety of techniques including STM.[1,9,27−63] STM-induced patterning of *n*-alkanethiol, $SH(CH)_nCH_3$, SAMs has generally been

* To whom correspondence should be addressed: e-mail, Crooks@chemvx.tamu.edu; voice, 409-845-5629; fax, 409-845-1399.

[⊗] Abstract published in *Advance ACS Abstracts,* March 15, 1997.

(1) Schoer, J. K.; Zamborini, F. P.; Crooks, R. M. *J. Phys. Chem.* **1996**, *100*, 11086−11091.
(2) Ulman, A. *An Introduction to Ultrathin Organic Films: from Langmuir-Blodgett to Self-Assembly*; Academic Press Inc.: San Diego, CA, 1991, and references therein.
(3) Dubois, L. H.; Nuzzo, R. G. *Annu. Rev. Phys. Chem.* **1992**, *43*, 437−463 and references therein.
(4) Bain, C. D.; Troughton, E. B.; Tao, Y.-T.; Evall, J.; Whitesides, G. M.; Nuzzo, R. G. *J. Am. Chem. Soc.* **1989**, *111*, 321−335 and references therein.
(5) Laibinis, P. E.; Whitesides, G. M.; Allara, D. L.; Tao, Y.-T.; Parikh, A. N.; Nuzzo, R. G. *J. Am. Chem. Soc.* **1991**, *113*, 7152−7167.
(6) Laibinis, P. E.; Whitesides, G. M. *J. Am. Chem. Soc.* **1992**, *114*, 1990−1995.
(7) Laibinis, P. E.; Whitesides, G. M. *J. Am. Chem. Soc.* **1992**, *114*, 9022−9028.
(8) Nuzzo, R. G.; Allara, D. L. *J. Am. Chem. Soc.* **1983**, *105*, 4481.
(9) Tiberio, R. C.; Craighead, H. G.; Lercel, M.; Lau, T.; Sheen, C. W.; Allara, D. L. *Appl. Phys. Lett.* **1993**, *62*, 476−478.
(10) Sheen, C. W.; Shi, J.-X.; Martensson, J.; Parikh, A. N.; Allara, D. L. *J. Am. Chem. Soc.* **1992**, *114*, 1514−1515.
(11) Lunt, S. R.; Santangelo, P. G.; Lewis, N. S. *J. Vac. Sci. Technol., B* **1991**, *9*, 2333−2336.
(12) Lunt, S. R.; Ryba, G. N.; Santangelo, P. G.; Lewis, N. S. *J. Appl. Phys.* **1991**, *70*, 7449−7467.
(13) Chailapakul, O.; Crooks, R. M. *Langmuir* **1993**, *9*, 884−888.
(14) Chailapakul, O.; Sun, L.; Xu, C.; Crooks, R. M. *J. Am. Chem. Soc.* **1993**, *115*, 12459−12467.
(15) Finklea, H. O.; Snider, D. A.; Fedyk, J. *Langmuir* **1990**, *6*, 371−376.
(16) Finklea, H. O.; Avery, S.; Lynch, M.; Furtsch, T. *Langmuir* **1987**, *3*, 409−413.
(17) Finklea, H. O.; Snider, D. A.; Fedyk, J. *Langmuir* **1993**, *9*, 3660−3667.
(18) Sabatani, E.; Rubinstein, I.; Maoz, R.; Sagiv, J. *J. Electroanal. Chem.* **1987**, *219*, 365−371.
(19) Sabatani, E.; Rubinstein, I. *J. Phys. Chem.* **1987**, *91*, 6663−6669.
(20) Miller, C. J.; Cuendet, P.; Gratzel, M. J. *J. Phys. Chem.* **1991**, *95*, 877−886.
(21) Strong, L.; Whitesides, G. M. *Langmuir* **1988**, *4*, 546−558.
(22) Singhe, R.; Whitesides, G. M. *J. Am. Chem. Soc.* **1990**, *111*, 7155.
(23) Bain, C. D.; Evall, J.; Whitesides, G. M. *J. Am. Chem. Soc.* **1989**, *111*, 7155−7164.
(24) Li, Y.-Q.; Chailapakul, O.; Crooks, R. M. *J. Vac. Sci. Technol.* **1995**, *B13*, 1300−1306.
(25) Schoer, J. K. *Electrochem. Soc. Interface* **1995**, *4*, 56−57.
(26) Crooks, R. M.; Chailapakul, O.; Ross, C. B.; Sun, L.; Schoer, J. K. In *Interfacial Design and Chemical Sensing*; Mallouk, T. E., Harrison, D. J., Eds.; American Chemical Society: Washington, DC, 1994; Vol. 561, pp 104−122.
(27) Wilbur, J. L.; Kumar, A.; Kim, A.; Whitesides, G. M. *Adv. Mater.* **1994**, *6*, 600.
(28) López, G. P.; Biebuyck, H. A.; Harter, R.; Kumar, A.; Whitesides, G. M. *J. Am. Chem. Soc.* **1993**, *115*, 10774−10781.
(29) López, G. P.; Biebuyck, H. A.; Whitesides, G. M. *Langmuir* **1993**, *9*, 1513−1516.
(30) Kumar, A.; Whitesides, G. M. *Appl. Phys. Lett.* **1993**, *63*, 2002−2004.
(31) Kumar, A.; Whitesides, G. M. *Science* **1994**, *263*, 60−62.
(32) Kumar, A.; Biebuyck, H. A.; Whitesides, G. M. *Langmuir* **1994**, *10*, 1498−1511.
(33) López, G. P.; Biebuyck, H. A.; Frisbie, C. D.; Whitesides, G. M. *Science* **1993**, *260*, 647−649.
(34) Kumar, A.; Biebuyck, H. A.; Abbott, N. L.; Whitesides, G. M. *J. Am. Chem. Soc.* **1992**, *114*, 9188−9189.
(35) López, G. P.; Albers, M. W.; Schreiber, S. L.; Carroll, R.; Peralta, E.; Whitesides, G. M. *J. Am. Chem. Soc.* **1993**, *115*, 5877−5878.
(36) Abbott, N. L.; Folkers, J. P.; Whitesides, G. M. *Science* **1992**, *257*, 1380.
(37) Abbott, N. L.; Whitesides, G. M.; Racz, L. M.; Szekely, J. *J. Am. Chem. Soc.* **1994**, *116*, 290−294.
(38) Abbott, N. L.; Kumar, A.; Whitesides, G. M. *Chem. Mater.* **1994**, *6*, 596−602.
(39) Abbott, N. L.; Rolison, D. R.; Whitesides, G. M. *Langmuir* **1994**, *10*, 2672.
(40) Lercel, M. J.; Rooks, M.; Tiberio, R. C.; Craighead, H. G.; Sheen, C. W.; Parikh, A. N.; Allara, D. L. *J. Vac. Sci. Technol., B* **1995**, *13*, 1139−1143.
(41) Lercel, M. J.; Craighead, H. G.; Parikh, A. N.; Sechadri, K.; Allara, D. L. *J. Vac. Sci. Technol., A* **1996**, *14*, 1844−1849.
(42) Lercel, M. J.; Redinbo, G. F.; Rooks, M.; Tiberio, R. C.; Craighead, H. G.; Sheen, C. W.; Allara, D. L. *Microelectron. Eng.* **1995**, *27*, 43−46.
(43) Gillen, G.; Wright, S.; Bennett, J.; Tarlov, M. J. *Appl. Phys. Lett.* **1994**, *65*, 534.

S0743-7463(96)00369-1 CCC: $14.00

accomplished by mechanical abrasion[59,60] or application of a high gap bias.[1,40,42,56−59,63] Numerous mechanisms have been proposed for STM-induced surface modification, including those based on electric fields, current, physical effects such as abrasion, as well as chemical and electrochemical processes.[1,64−69] Identification of a specific mechanism (or mechanisms) is a difficult analytical problem for three reasons. First, the size scale of the patterning precludes far-field optical microscopic or spectroscopic analysis. Second, it is difficult to vary individual experimental parameters while holding all others constant. For example, it is impossible to independently control the tunneling current, gap bias, and tip−sample separation. Third, multiple sequential or simultaneous mechanisms may be responsible for patterning.

We previously demonstrated that patterning an *n*-alkanethiol SAM with a stationary STM tip only occurred if a bias threshold of ∼+2.3 V was exceeded. Further, patterning of methyl-terminated SAMs with a scanning tip did not occur at relative humidity (RH) <∼25% at biases up to 5.0 V. Finally, fabrication of complete patterns only occurred at RH >∼70%. On the basis of these results, we proposed a model for SAM removal based on faradaic electrochemistry.[1]

Here we propose a more detailed model, illustrated in Chart 1, that is consistent with our previous findings and those presented here. The *n*-alkanethiol SAM is initially well-organized and effectively passivates the surface (frame 1). In the first patterning step (frame 2) the STM tip interacts with the SAM causing local disruption of the order within the monolayer, reducing the cohesion energy of individual molecules, and destabilizing the SAM.[70−72]

Under low bias (≤∼+2.3 V) conditions, or when patterning at low RH (<∼25%) at biases <∼+5.0 V, removal or redistribution of the SAM and substrate is very slow. However, the level of monolayer disruption is still sufficient to allow penetration of adventitious adsorbates or lithographic debris into the SAM which in turn impede relaxation of the SAM back to its preimaged structure and make the monolayer vulnerable to further patterning or electrochemistry (frame 3a). Intercalation of adventitious adsorbates or lithographic debris is consistent with reports indicating that the solvent used during casting, analysis, or modification of a SAM can be incorporated into the monolayer, thereby hindering adsorption of the SAM, or otherwise influencing its physical and chemical properties.[2,4,22,23,73−76]

If the events described above are accompanied by a tip-substrate bias of ∼+2.3 to ∼+3.0 V at RH >25%, the combination of the bias, humidity, and locally disrupted monolayer results in controlled removal of the SAM by faradaic electrochemical processes (Frame 3b).[1] We are uncertain of the specific electrochemical reactions that occur but have previously suggested that oxidation of the thiol may figure prominently.[1] Patterning generates lithographic debris consisting of SAM fragments, adventitious adsorbates, and probably some Au, in the patterned feature and on the tip. This debris can be removed by repeated scanning within the pattern at low bias (frame 4).

Experimental Section

Chemicals. *n*-Octadecyl mercaptan (ODM), $HS(CH_2)_{17}CH_3$ (Aldrich, 98%), and 100% ethanol were used as received.

Sample Preparation. All substrates were Au balls prepared from ∼2 cm lengths of Au wire (0.25 mm diameter, 99.9985% purity, Johnson Matthey; or 0.50 mm diameter, 99.985%, Sigmund Cohen) as previously described.[1,13,26,56,57,77−82] Except as noted, the substrates were immersed in ethanolic solutions of ODM (∼2.0 mM) for 16−24 h, removed from solution, rinsed with absolute ethanol, and dried under a gentle stream of N_2. This procedure has previously been shown to yield well-ordered, close-packed SAMs that effectively passivate the surface.[13,26,56,57]

STM Data Acquisition. A NanoScope III STM (Digital Instruments, Santa Barbara, CA) was used for all experiments. Tips were mechanically cut from Pt/Ir wire (80/20%, Ted Pella) and substrates were mounted into a custom holder.[1] The STM *z*-piezo was calibrated by measuring Au(111) monatomic step edges and correlating the mean measured value to the calculated Au(111) interlayer spacing of 0.235 nm as previously described.[83] Unless otherwise noted, all images were obtained in air using a D scanner (∼12 μm lateral scan range) under ambient humidity conditions, which typically vary between 40% and 70%. Tun-

(44) Chan, K. C.; Kim, T.; Schoer, J. K.; Crooks, R. M. *J. Am. Chem. Soc.* **1995**, *117*, 5875−5876.
(45) Dressick, W. J.; Calvert, J. M. *Jpn. J. Appl. Phys.* **1993**, *32*, 5829.
(46) Li, Y.; Huang, J.; McIver, R. T. J.; Hemminger, J. C. *J. Am. Chem. Soc.* **1992**, *114*, 2428−2432.
(47) Huang, J.; Hemminger, J. C. *J. Am. Chem. Soc.* **1993**, *115*, 3342−3343.
(48) Huang, J.; Dahlgren, D. A.; Hemminger, J. C. *Langmuir* **1994**, *10*, 626−628.
(49) Tarlov, M. J.; Newman, J. G. *Langmuir* **1992**, *8*, 1398−1405.
(50) Tarlov, M. J.; Burgess, D. R. F., Jr.; Gillen, G. *J. Am. Chem. Soc.* **1993**, *115*, 5305−5306.
(51) Wollman, E. W.; Frisbie, C. D.; Wrighton, M. S. *Langmuir* **1993**, *9*, 1517−1520.
(52) Wollman, E. W.; Kang, D.; Frisbie, C. D.; Lorkovic, I. M.; Wrighton, M. S. *J. Am. Chem. Soc.* **1994**, *116*, 4395−4404.
(53) Graham, R. L.; Bain, C. D.; Biebuyck, H. A.; Laibinis, P. E.; Whitesides, G. M. *J. Phys. Chem.* **1993**, *97*, 9456−9464.
(54) Laibinis, P. E.; Graham, R. L.; Biebuyck, H. A.; Whitesides, G. M. *Science* **1991**, *254*, 981−983.
(55) Marrian, C. R. K.; Perkins, F. K.; Brandow, S. L.; Koloski, T. S.; Dobisz, E. A.; Calvert, J. M. *Appl. Phys. Lett.* **1994**, *64*, 390.
(56) Ross, C. B.; Sun, L.; Crooks, R. M. *Langmuir* **1993**, *9*, 632−636.
(57) Schoer, J. K.; Ross, C. B.; Crooks, R. M.; Corbitt, T. S.; Hampden-Smith, M. J. *Langmuir* **1994**, *10*, 615−618.
(58) Corbitt, T. S.; Crooks, R. M.; Ross, C. B.; Hampden-Smith, M. J.; Schoer, J. K. *Adv. Mater.* **1993**, *5*, 935−938.
(59) Kim, Y.-T.; Bard, A. J. *Langmuir* **1992**, *8*, 1096−1102.
(60) Kim, Y.-T.; McCarley, R. L.; Bard, A. J. *Langmuir* **1993**, *9*, 1941−1944.
(61) Edinger, K.; Gölzhäuser, A.; Demota, G. K.; Wöll, C.; Grunze, M. *Langmuir* **1993**, *9*, 4−8.
(62) Demir, U.; Balasubramanian, K. K.; Cammarata, V.; Shannon, C. *J. Vac. Sci. Technol., B* **1995**, *13*, 1294−9.
(63) Lercel, M. J.; Redinbo, G. F.; Craighead, H. G.; Sheen, C. W.; Allara, D. L. *Appl. Phys. Lett.* **1994**, *65*, 974−976.
(64) Stroscio, J. A.; Eigler, D. M. *Science* **1991**, *254*, 1319−1326 and references therein.
(65) Staufer, U. In *Scanning Tunneling Microscopy II*; Wiesendanger, R., Güntherodt, J., Eds.; Springer-Verlag: New York, 1992; Vol. 28, pp 273−302 and references therein.
(66) Parkinson, B. In *Supramolecular Architecture: Synthetic Control in Thin Films and Solids*; Bein, T., Ed.; American Chemical Society: Washington, DC, 1992; Vol. 499, pp 76−85 and references therein.
(67) Quate, C. F. *Springer Ser. Solid State Sci.* **1992**, *111* (Low Dimensional Electronic Systems), 85−96 and references therein.
(68) *Scanning Tunneling Microscopy and Spectroscopy: Theory, Techniques and Applications*; Bonnell, D. A., Ed.; VCH: New York, 1993; pp 1−436 and references therein.
(69) *Scanning Tunneling Microscopy*; Stroscio, J. A., Kaiser, W. J., Eds.; Academic Press: London, 1993; Vol. 27, pp 1−459 and references therein.
(70) Sellers, H.; Ulman, A.; Shnidman, Y.; Eilers, J. E. *J. Am. Chem. Soc.* **1993**, *115*, 9389.
(71) Thomas, R. C.; Houston, J. E.; Crooks, R. M.; Kim, T.; Michalske, T. A. *J. Am. Chem. Soc.* **1995**, *117*, 3830−3834.
(72) Thomas, R. C. Ph.D. Dissertation, The University of New Mexico, 1994.
(73) Bartell, L. S.; Betts, J. F. *J. Phys. Chem.* **1960**, *64*, 1075−1076.
(74) Bewig, K. W.; Zisman, W. A. *J. Phys. Chem.* **1963**, *67*, 130−135.
(75) Levine, O.; Zisman, W. A. *J. Phys. Chem.* **1957**, *61*, 1188−1196.
(76) Schneider, T. W.; Buttrey, D. A. *J. Am. Chem. Soc.* **1993**, *115*, 12391−12397.
(77) Sun, L.; Crooks, R. M. *J. Electrochem. Soc.* **1991**, *138*, L23−L25.
(78) Snyder, S. R. *J. Electrochem. Soc.* **1992**, *139*, 5C.
(79) Hsu, T. *Ultramicroscopy* **1983**, *11*, 167−172.
(80) Hsu, T.; Cowley, J. M. *Ultramicroscopy* **1983**, *11*, 239−250.
(81) Schmidt, L. D. *CRC Crit. Rev. Solid State Mater. Sci.* **1978**, *7*, 129−141.
(82) Gwathmey, A. T.; Cunningham, R. E. *Adv. Catal.* **1958**, *10*, 57−95.
(83) Sun, L.; Crooks, R. M. *Langmuir* **1993**, *9*, 1951−1954.

Chart 1

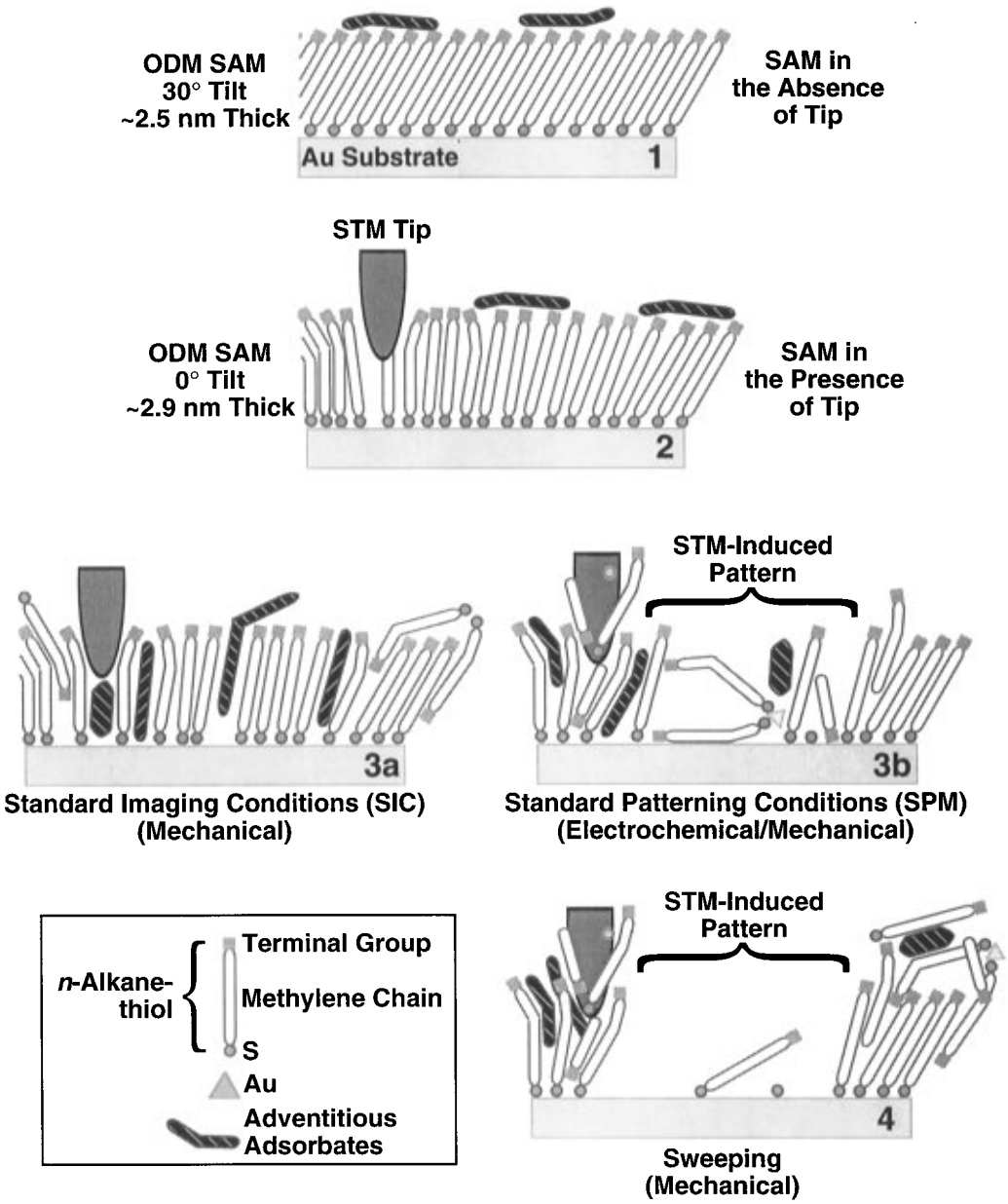

neling conditions during imaging were selected to minimize tip-induced surface damage: +0.3 V sample bias (positive voltages indicate that the substrate is positive relative to the tip), 150 pA tunneling current, scan rates between 2.0 and 5.0 Hz, and 256 × 256 pixel resolution.[84,85] We refer to these as standard imaging conditions (SIC) in the text. To further minimize tip-induced surface damage, each region was imaged a minimum number of times, typically five or fewer scans.

STM-Induced Patterning. Except as noted, patterns were fabricated using +3.0 V bias, 150 pA tunneling current, 41 Hz scan rate, and 256 × 256 pixel resolution. We refer to these as standard patterning conditions (SPC) in the text. Patterns were typically 50 nm × 50 nm and fabricated by scanning four times using SPC in air (unless otherwise noted).

To characterize the patterns, we examined images of the surface before, during, and after patterning for changes in the general appearance of indigenous surface features, depth and lateral dimensions of STM-induced patterns, and root-mean-square (rms) roughness of the surface and patterns. Prior to obtaining measurements, each image was planefit and flattened to eliminate most imaging artifacts. "Stop bands" were then used to electronically crop each image to remove any remaining imaging artifacts and Au terraces different from that on which the patterns was formed.

The roughness analysis function of the NanoScope software was used to measure the pattern depth,[86] the rms roughness of the pattern,[87] and the rms roughness of the unpatterned surface. The reported pattern depth is the absolute value of the difference between the mean levels of the plane of the pattern and the adjacent unpatterned terrace. To partially account for variability between images and to provide a more useful comparison of changes in the surface roughness, we calculated an rms roughness factor (RRF) by normalizing the rms roughness of the primary

(84) Schoer, J. K.; Ross, C. B.; Sun, L.; Crooks, R. M. Unpublished results.

(85) In a previous publication (ref 56) we indicated that scanning the surface with these mild conditions could lead to rapid modification of the surface. The sample from which we obtained the data in Figure 1 of ref 56 had been exposed to Cu underpotential deposition (UPD) and cyclic voltammetry prior to scanning by STM. As a result, the SAM had been disrupted before the STM images were obtained. Interestingly, this method may have future utility for facilitating the patterning.

(86) The Nanoscope software calculates the mean feature level in the roughness analysis feature by calculating the average of all the z values within a selected area relative to the z value of the tip when it engages the surface.

(87) The NanoScope software defines the rms Roughness (R_q) as $R_q = \{[\sum(Z_i - Z_{ave})^2]/N\}^{1/2}$, where Z_i is the individual height of the pixel and Z_{ave} is the average height of the N pixels over which the calculation is performed.

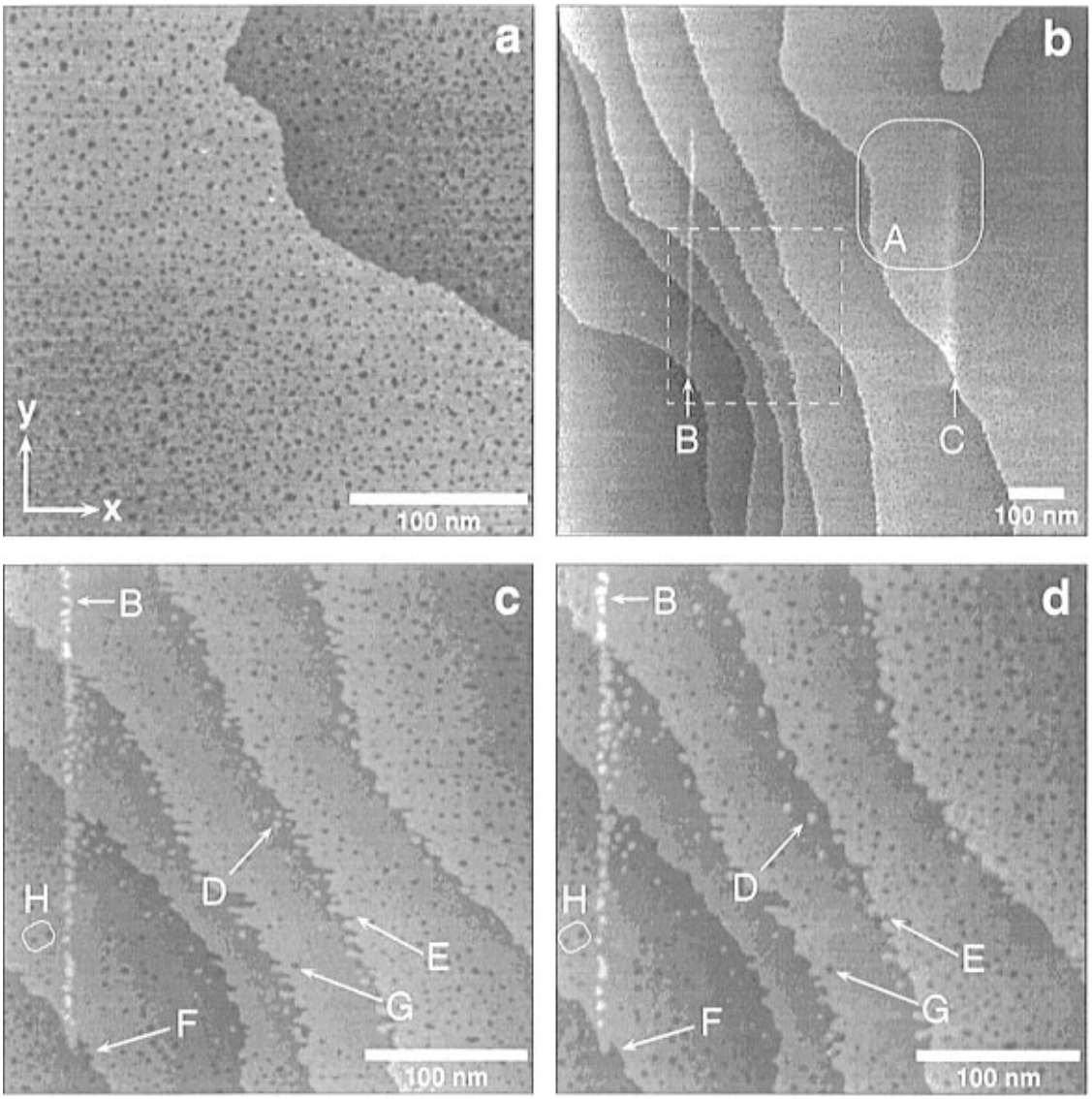

Figure 1. A series of STM images illustrating (a) an unpatterned ODM-coated Au(111) surface and (b−d)the types of tip-induced modification that can occur after scanning across a highly terraced region with high tip velocity or imaging the same region for prolonged time periods using standard imaging conditions (SIC). (b) STM image obtained after scanning the central 500 nm × 500 nm area four times with SIC, except the scan rate was 41 Hz to accelerate tip-induced modification. (c) STM image of the region enclosed by the dashed box in (b). (d) STM image of the region shown in (c) after scanning the same area with SIC for more than 3.5 h. The gray scale is 2 nm in all images.

pattern (*vide infra*) or, in the case of prepattern surfaces the area to be patterned, to the rms roughness of the surrounding unpatterned terrace.[88] The RRF of the unpatterned surface typically ranges from 0.7 to 1.1.

Results and Discussion

Standard Imaging Conditions (SIC). Figure 1a is a 300 nm × 300 nm image of an unpatterned ODM-coated Au surface that is typical of those acquired using SIC. The image is characterized by two atomically flat terraces covered by randomly distributed pits 0.24 nm deep and 2−5 nm in diameter. The pits are indigenous to organomercaptan-coated Au surfaces and result from SAM-induced restructuring of the Au substrate.[14,61,89−92] The key points are that these defects are in the Au surface and filled with organized organomercaptans and thus do not represent molecular vacancies in the SAM.

Figure 1b is a 1 μm × 1 μm image obtained after scanning the central 500 nm × 500 nm of the imaged area four times using standard imaging conditions (SIC, see experimental Section for details) except that the scan rate was more rapid (41 Hz). We intentionally chose these conditions and a location on the surface with numerous closely-spaced terrace edges to accelerate any surface modification that may occur when using these non-aggressive conditions. Such modification can take several forms. Region A is representative of a region within a scanned area that appears slightly elevated (0.01 nm).[93,94] Electrochemical scanning tunneling microscopy (ECSTM) results indicate that regions on the surface that appear

(88) We define the rms roughness factor (RRF) as RRF = (rms roughness of patterned area)/(rms roughness of the SAM-modified unpatterned Au(111) terrace).

(89) Schönenberger, C.; Sondag-Huethorst, J. A. M.; Jorritsma, J.; Fokkink, L. G. J. *Langmuir* **1994**, *10*, 611−614.

(90) McCarley, R. L.; Dunaway, D. J.; Willicut, R. J. *Langmuir* **1993**, *9*, 2775−2777.

(91) Bucher, J.-P.; Santesson, L.; Kern, K. *Langmuir* **1994**, *10*, 979−983.

(92) Poirier, G. E.; Tarlov, M. J. *Langmuir* **1994**, *10*, 2853−2856.

(93) We also occasionally observe this type of behavior after patterning large features (≥500 nm × 500 nm) with biases ≤∼3.5 V, when patterning the surface in low humidity environments, and we frequently observe this behavior when working in solution (ref 94).

(94) Schoer, J. K.; Ross, C. B.; Sun, L.; Zamborini, F. P.; Li, Y.; Chailapakul, O.; Crooks, R. M. Unpublished results.

elevated after being scanned with an STM tip do not passivate the Au surface toward electrochemical etching with cyanide as effectively as unpatterned SAMs (see Supporting Information). As a result, we believe that the elevated regions represent an early stage of SAM patterning, as shown in Chart 1, Frame 3a, which is a consequence of STM tip penetration into the SAM. Arrows B and C indicate ridges, which are probably composed of organomercaptans, organomercaptan fragments, adventitious adsorbates, and a small amount of Au, that are clearly visible at the edges of this slightly modified region.

Figure 1c is an image of the region defined by the dashed line in Figure 1b. This region encompasses the lower-left corner of the area scanned at high tip velocity and also part of the unmodified surface. Ridge B is now resolved as a series of islands with typical in-plane dimensions of 2−30 nm. Erosion of the step edges occurs only inside the area previously scanned at 41 Hz. Erosion takes the form of 2−10 nm diameter islands isolated from the adjacent terrace (feature D) and serrations 2−20 nm in length (feature E), which result from indigenous pits expanding to become part of the terrace edge.

Figure 1d was obtained after scanning the region depicted in Figure 1c for more than 3.5 h using SIC. The small islands (feature D) aggregate into larger islands and merge with ridge B. Features such as B and D are resistant to removal by the scanning action of the tip, implying that the islands and ridges are not simply physisorbed to the surface but are bound or intercalated into the SAM as shown in frame 3a of Chart 1. Smoothing of terrace edges (features E and F) and slight broadening of indigenous pits both inside and outside the area previously scanned with high tip velocity (features G and H, respectively) are also visible. However, we have not observed any increase in the depth of the indigenous pits when using SIC, and there is essentially no change in the measured rms surface roughness. Images of adjacent portions of the surface obtained after Figure 1d are similar to that of Figure 1a, confirming that the effects seen in Figure 1d are not the result of tip degradation. These results demonstrate that an unpatterned ODM SAM can be very slowly modified using SIC and are in general accord with previous observations.[60,90]

Our results are reminiscent of those in recent reports, which showed that heating an *n*-alkanethiol-coated substrate to >350 K anneals the surface by eliminating indigenous pits and, after initially causing serrated step edges, eventually smoothing terrace edges.[90,91,95] The annealing has been attributed to thermally activated diffusion of Au[90] or a mobile Au−mercaptan complex.[95] A similar annealing phenomenon may be operative here, except that it is induced by the STM tip.

Unlike using SIC to image an unpatterned surface, scanning within a previously fabricated pattern using SIC increases the pattern depth significantly during the first few (approximately four) scans (see Supporting Information), after which the depth remains approximately constant (frame 4 of Chart 1). Also during this time the RRF steadily decreases and eventually approaches its prepatterning value. These results indicate that loosely bound material is present inside the pattern after fabrication and that material is removed and redistributed by scanning within a pattern. Thus, intact SAMs suffer only minor tip-induced topographical changes, but SAMs that are intentionally disrupted are susceptible to further structural changes even when tip conditions are nonaggressive.

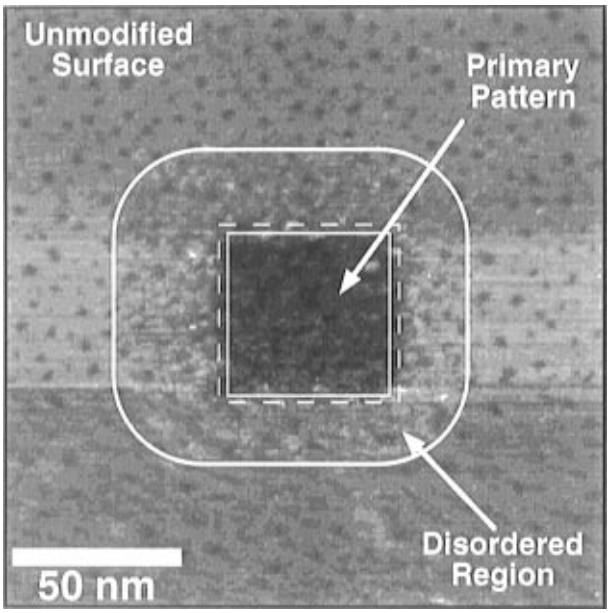

Figure 2. STM image showing the key features of an ODM-coated Au(111) surface after fabrication of a nominally 50 nm × 50 nm pattern fabricated using standard patterning conditions (SPC) and four scans. The gray scale is 2 nm.

Standard Patterning Conditions, General Pattern Characteristics. We can identify four unique regions on a surface after patterning using standard patterning conditions (SPC, see Experimental Section for details). These are delineated in Figure 2. The first region is the unmodified part of the surface. Located outside the white oval, it is characterized by an intact, unmodified SAM. The light gray areas to the left and right of the pattern are imaging artifacts that result from the time response of the piezoelectric scanner.

The second region, located inside the solid square, is the primary pattern where most of the SAM has been removed. Two other regions are of interest for describing pattern fabrication and determining the resolution limits of this method. There is a region ∼5 nm wide between the dashed and solid squares, which we call the "extended" primary pattern. It results from a combination of microscope drift during patterning[96] and the electrochemical nature of SAM removal.[1] Because we are unable to identify any differences in the properties of the primary and extended patterns, we treat them hereafter as a single "primary" pattern.

The fourth distinct region, which we term the "disordered" region, is located between the oval and dashed square. This area is characterized by apparent disordering of the surface beyond the primary pattern. The size, shape, and position of the disordered region relative to the primary pattern is constant for a specific set of experimental conditions but is generally not symmetrical about the primary pattern. For example, in Figure 2 the disordered region extends ∼30 nm beyond the primary pattern but is displaced left of center.

It is important to recognize that during patterning the disordered region is not scanned by the portion of the tip responsible for fabricating the primary pattern. Therefore the disordered region results from a long-range interaction between the tip and surface, which we have previously shown to arise from a faradaic electrochemical process.[1] Consistent with this model, the dimensions of the disordered region decrease with decreasing RH: at very high

(95) Delamarche, E.; Michel, B.; Kang, H.; Gerber, C. *Langmuir* **1994**, *10*, 4103−4108.

(96) We typically observe less than 2 nm of drift during 4 patterning scans at 41 Hz scan rate and 256 × 256 pixel resolution (about 25 s).

humidities (>∼80%) the disordered region can extend for hundreds of nanometers, while at low humidities it is absent.

We believe that the structural damage apparent in the disordered region represents an intermediate stage of patterning such as partial removal, oxidation, or cleavage of the SAM (Chart 1, Frames 2, 3a, and 3b), which in turn reduces its passivating ability and disrupts intermolecular van der Waals interactions within the monolayer. Since the most thermodynamically favored state for *n*-alkanethiols on Au(111) is a close-packed monolayer, *n*-alkanethiol molecules in the disordered region will rearrange themselves to re-establish this highly-ordered state. Consistent with this hypothesis, our studies of pattern stability show that in the absence of a scanning tip the disordered region coalesces into discrete islands and terraces (see Supporting Information). However, the depth, rms roughness, and lateral dimensions of the primary pattern decrease only slightly even after 95 h in ambient. Similarly, the unpatterned surface does not change. Additionally, *in-situ* electrochemical STM experiments show that electrochemically induced dissolution of Au by CN^- selectively dissolves Au from both the primary pattern and disordered region while leaving the unmodified SAM surface intact (see Supporting Information). These results are consistent with our proposed model, but they imply that the ultimate resolution of STM lithography, at least under the conditions employed here, is limited by the dimensions of the disordered region, rather than by the dimensions of individual molecules.

It has been established that material can be transferred between a substrate and STM tip,[97−99] and Figure 2 provides evidence that some of the debris is transferred to the tip in our experiment. The slow-scan direction of the tip in this image was from top to bottom. Note that the indigenous pits at the top of the image and most of the STM-induced pattern are well-resolved. However, after the tip has almost reached the bottom of the image, the pattern resolution is degraded. Similar resolution changes in other images virtually always occur as the tip is scanning across a pattern, but not when scanning unpatterned portions of the surface. We attribute the degradation of image quality to debris from the patterned area transferring from the surface to the tip.[100]

Standard Patterning Conditions, Effect of Bias. We previously established that when a bias pulse is applied to a stationary tip, no patterning occurs regardless of the current (up to at least 10 nA) unless the tip−sample gap bias exceeds a critical threshold value of ∼+2.3 V.[1] We observe a similar effect when patterning with a scanning tip (see Supporting Information). An electrochemical patterning model predicts this potential dependence and also our observation that once the bias threshold is exceeded the pattern dimensions will increase as the magnitude of the bias and the Coulomb dose increase.

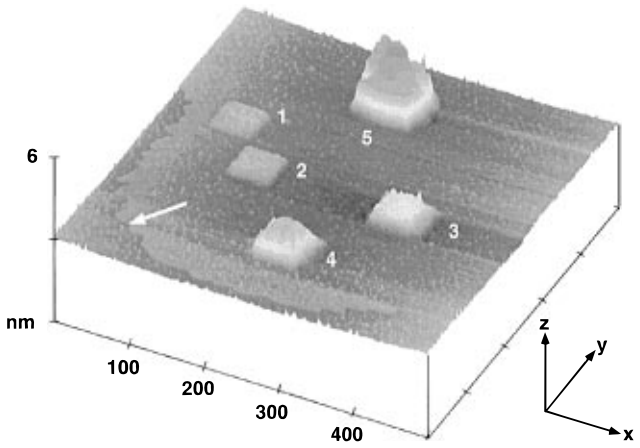

Figure 3. An inverted, three-dimensional rendering of an STM image of an ODM SAM surface obtained after the formation of five nominally 50 nm × 50 nm patterns (seen in the figure as mounds) fabricated using SPC except for the conditions listed in Table 1.

Figure 3 is an inverted, three-dimensional rendering of an ODM SAM surface after fabrication of five nominally 50 nm × 50 nm patterns using SPC except as noted in Table 1. Table 1 also contains data describing the physical characteristics of the patterns. The data for features 1, 3, and 5 clearly show the expected increase in the depth, width, and roughness of patterns as the bias used during fabrication increases. Biases of ≤∼+3.0 V (features 1 and 2) lead to well-defined patterns. Patterns fabricated at +3.5 V (features 3 and 4) yield well-defined pattern edges, but the magnitude and variability of the RRF and depth are significantly larger than those prepared at +3.0 V. These trends continue and are exacerbated at even higher patterning biases so that patterns fabricated using biases ≥∼+4.0 V (feature 5) are generally irreproducible (i.e., the pattern depth, shape, lateral dimensions, and rms roughness cannot be reliably predicted).

Standard Patterning Conditions, Effect of Coulomb Dose. Figure 4 shows four patterns fabricated with SPC except the tip current was increased as noted in Table 2. Table 2 also contains data describing the physical characteristics of the patterns. There is a clear increase in the depth and width of the patterns as the current (Coulomb dose) increases, which is consistent with either the proposed electrochemical mechanism or a mechanism that relies on energy transfer from a high-energy electron beam to the surface. However, if the primary patterning mechanism is not electrochemical, the patterning would be independent of the ambient relative humidity. Because our previous report demonstrated that patterning does not occur at biases up to 5.0 V at low relative humidities and that the patterning threshold is independent of the current, we can eliminate electron-beam damage as the primary patterning mechanism at biases ≤∼+3.0 V.

An alternative approach to increasing the Coulomb dose is to increase the number of scans used to pattern the surface while keeping the current constant. Figure 5 and Table 3 illustrate the impact of repeatedly patterning a nominally 50 × 50 nm pattern into an ODM-coated Au(111) surface using SPC. Parts a−d of Figure 5 are images obtained after 1, 10, 60, and 250 patterning cycles, respectively. The images have been inverted and displayed in three dimensions to emphasize the pattern depth. Clearly, increasing the Coulomb dose by repetitively patterning the surface using SPC results in a progressive increase in pattern depth (feature A), which is consistent with an electrochemical patterning mechanism. The grooves that are apparent on either side of

(97) *Scanning Tunneling Microscopy II*; Wiesendanger, R., Güntherodt, H.-J., Eds.; Springer-Verlag: Heidelberg, 1992; Vol. 28, pp 1−308 and references therein.

(98) *Scanning Tunneling Microscopy and its Applications*; Bai, C., Ed.; Springer-Verlag: Heidelberg, 1992; Vol. 32, pp 1−331 and references therein.

(99) Chen, C. J. *Introduction to Scanning Tunneling Microscopy*; Oxford University Press: New York, 1993; pp 1−412 and references therein.

(100) These types of changes in the imaging ability of the tip can frequently be eliminated by pulsing the bias to +3 to +4 V for <1 s. These brief pulses generally result in the formation of a mound(s) on the surface, suggesting that material is transferred from the tip to the surface.

Table 1. Summary of the Critical Parameter Values Employed To Fabricate the Features in Figure 3 and the Physical Characteristics of the Resulting Features

feature	patterning bias (V)	no. of patterning scans	*x*-width (nm)	*y*- width (nm)	*z*-depth[a] (nm)	RRF[b]
1	3.0	4	58	57	0.21	1.5
2	3.0	8	60	60	0.22	1.4
3	3.5	4	73	61	0.75	3.4
4	3.5	8	69	72	1.23	5.3
5	4.0	4	84	80	2.78	12.3
background						0.1[c]
step edge					0.24	

[a] The absolute value of the difference in the *z*-values between the plane of the pattern and the plane of the unpatterned SAM-coated Au(111) terrace. [b] The RRF is the rms roughness of the central 50 nm × 50 nm of the primary pattern divided by the rms roughness of the surrounding unpatterned terrace. [c] This value is the rms roughness value for the background, to provide some idea of the absolute numbers for the roughness of the patterns.

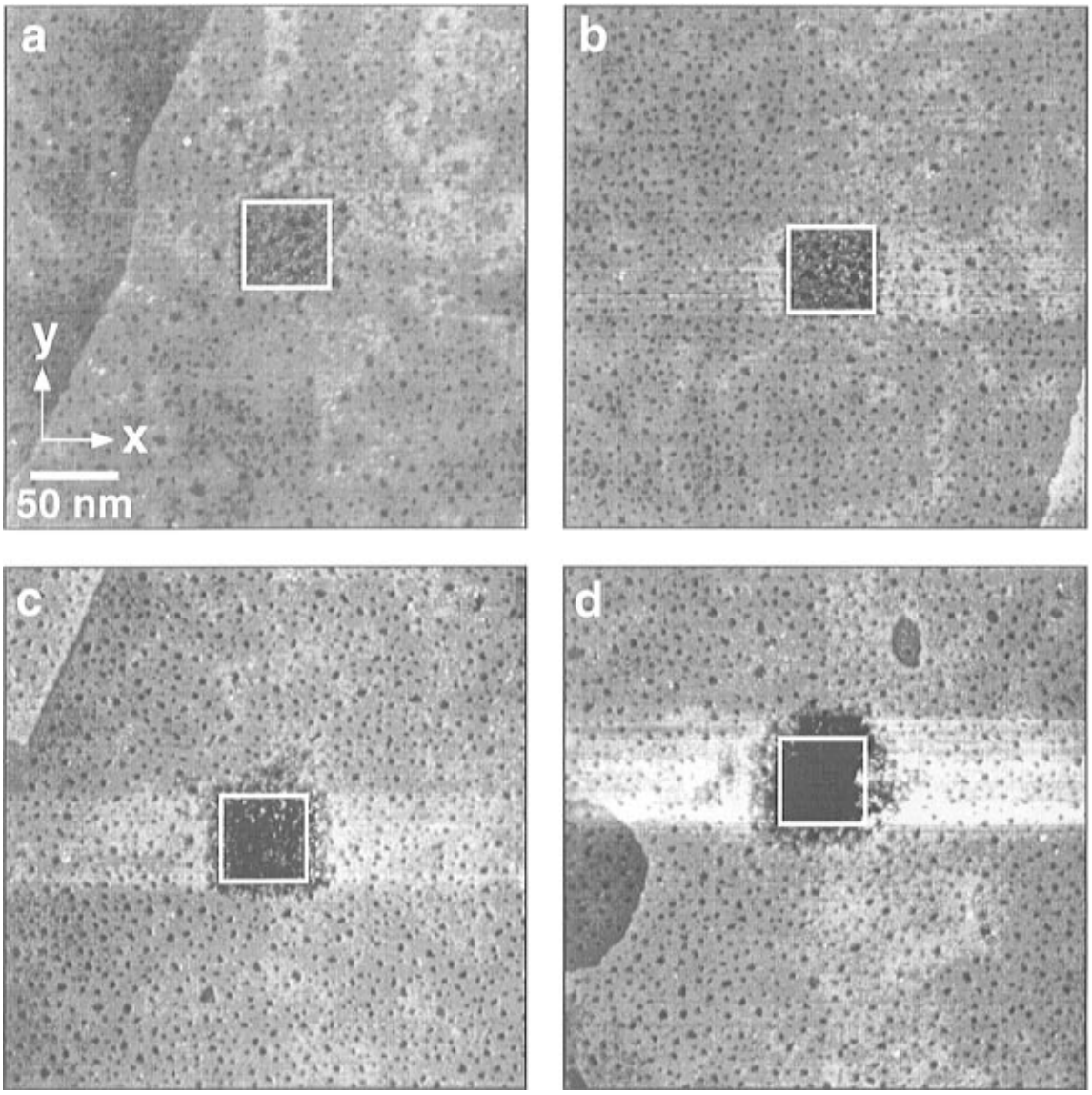

Figure 4. STM images of four patterns fabricated on an ODM-coated Au(111) surface in air using SPC while varying the tunneling current. The tunneling current was (a) 0.030 nA, (b) 0.150 nA, (c) 1.5 nA, and (d) 6.0 nA, respectively. The gray scale is 2 nm. Table 2 lists some physical characteristics of the patterns.

the pattern (feature B in Figure 5d) result from instrumental artifacts discussed earlier. Consistent with formation of a highly resistive, ultrathin electrochemical cell adjacent to the tip, the *x*- and *y*-dimensions of the primary pattern also increase slightly as the number of patterning scans increases, reaching 60 and 58 nm, respectively, after 250 patterning scans.

Indigenous pits in the Au are easily identified within the patterned area in Figure 5a, and even after 10 scans at +3.0 V (Figure 5b) they are still visible. These pits are generally observed when patterns are fabricated using these conditions and strongly suggest that the patterning is restricted primarily to the SAM during at least the initial 10−12 scans.

A disordered region (feature C) is visible around the primary pattern after 10 scans (Figure 5b). Consistent with the disordered region representing an early stage of patterning, both the lateral dimensions and depth of the

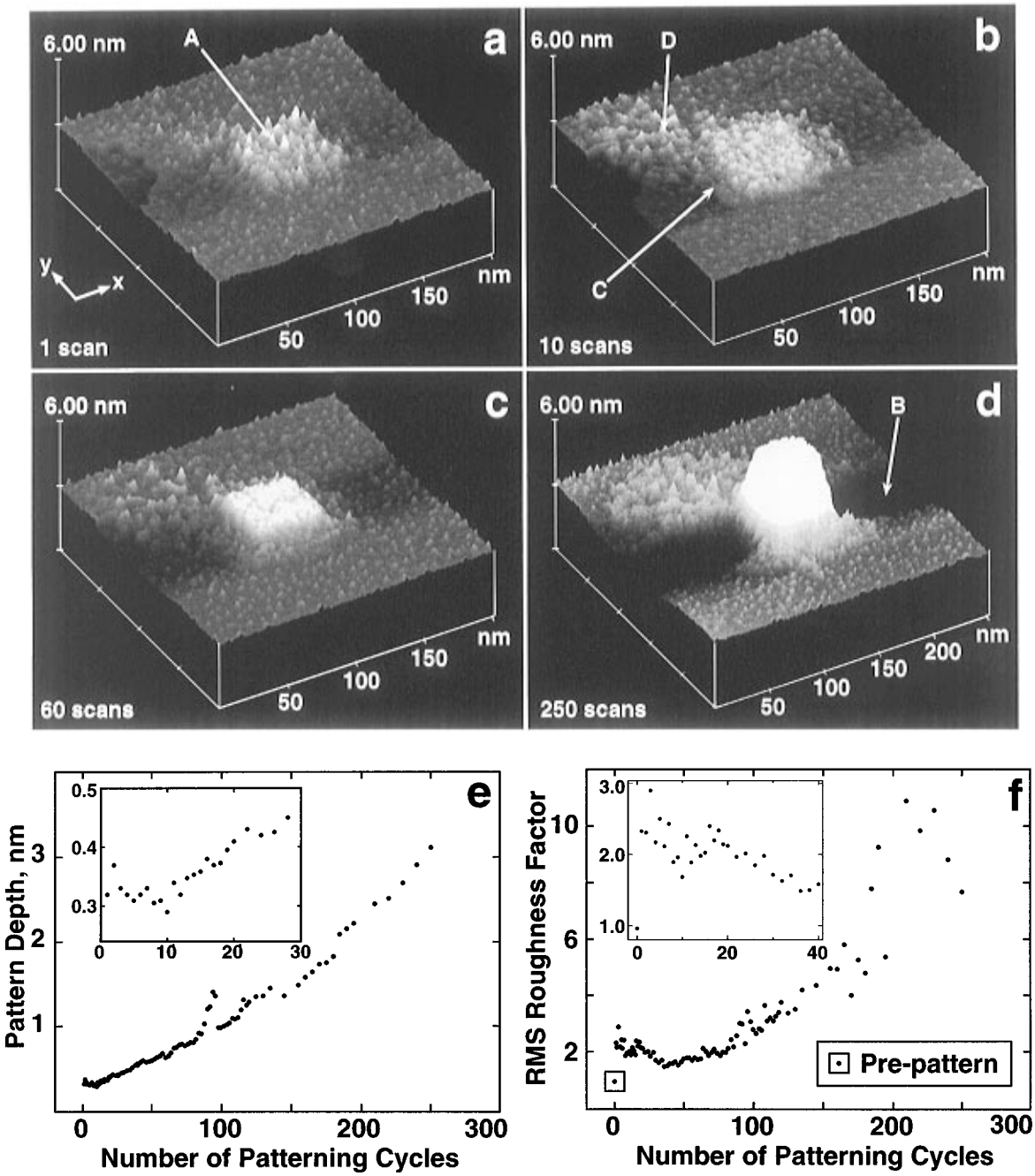

Figure 5. Images showing the effect of increasing the Coulomb dose per unit area by repetitively scanning a nominally 50 nm × 50 nm area on an ODM-coated Au(111) surface using SPC. The images were obtained after (a) 1, (b) 10, (c) 60, and (d) 250 patterning scans. The images are inverted and displayed in three dimensions to emphasize the pattern dimensions. Table 3 lists some physical characteristics of the pattern. (e) Plot of the pattern depth as a function of the number of patterning scans. The inset shows the results of the first 28 patterning scans. (f) Plot of the RRF as a function of the number of patterning scans. The inset shows the results of the first 40 patterning scans.

disordered region increase as the number of patterning cycles increase. The formation of a secondary pattern (feature D) is also visible in Figure 5b−d. Both the primary and secondary patterns have similar lateral dimensions, but as shown in parts c and d of Figure 5 the depth of the secondary pattern is not as great as the primary pattern. The secondary pattern is likely the result of a second protrusion on the tip that is in close proximity to the surface. The presence of a secondary pattern has important implications for the use of arrays of STM tips for micro- and nanofabrication. Our data illustrate that it is possible to use multiple tips to pattern a surface; however, the data also underscore the impact of imprecisely aligned tips within an array.

As shown in Figure 5e, the primary pattern depth remains approximately constant at ∼0.32 nm during the first 10−12 patterning scans. Figure 5f shows that during this same period the RRF decreases, indicating that repetitive scanning within a pattern (even with SPC) initially smoothes the pattern bottom. These results indicate that lithographic debris must be physically removed from or redistributed within the pattern by the tip before the surface is sufficiently exposed that the pattern depth can again increase (Chart 1, frames 3b and 4). Consistent with an electrochemical desorption mechanism, the pattern depth increases approximately linearly after the first 10−12 scans. Additionally, the indigenous pits also start to become obscured after 10−12 scans,

Table 2. Summary of the Critical Parameter Values Employed To Fabricate the Features in Figure 4 and the Physical Characteristics of the Resulting Features

figure	patterning current (nA)	*x*-width (nm)	*y*-width (nm)	*z*-depth[a] (nm)	RMS roughness (nm)	RRF[b]
4a	0.03	53	52	0.23	0.15	1.1
4b	0.15	55	56	0.42	0.39	1.5
4c	1.5	55	57	0.81	0.44	2.1
4d	6.0	58	63	1.66	0.83	4.6

[a] The absolute value of the difference in the *z*-values between the plane of the pattern and the plane of the unpatterned SAM-coated Au(111) terrace. [b] The RRF is the rms roughness of the central 50 nm × 50 nm of the primary pattern divided by the rms roughness of the surrounding unpatterned terrace.

Table 3. Physical Characteristics of the Pattern Shown in Figure 5 as a Function of the Number of Patterning Scans Using Standard Patterning Conditions, SPC

no. of patterning scans	unpatterned terrace RMS roughness (nm)	primary pattern		
		z-depth (nm)[a]	RMS roughness (nm)	RMS roughness factor[b]
Pre-pattern	0.08	0.00	0.08	1.0
1	0.07	0.32	0.16	2.3
10	0.06	0.30	0.11	1.7
60	0.07	0.62	0.12	1.7
250	0.10	3.09	0.75	7.7

[a] The absolute value of the difference in the *z*-values between the plane of the pattern and the plane of the unpatterned SAM-coated Au(111) terrace. [b] The RRF is the rms roughness of the central 50 nm × 50 nm of the primary pattern divided by the rms roughness of the surrounding unpatterned terrace.

suggesting that the Au substrate begins to be patterned at this point. After 250 patterning scans using SPC, the pattern depth reaches ∼3.1 nm, a value substantially greater than the thickness of the ODM monolayer (∼2.5 nm), which clearly indicates that the pattern is well into the Au substrate.

The dwell time of the tip per unit area per scan is controlled by the scan rate, scan size, and image resolution. By simultaneously varying these parameters while maintaining constant gap bias and tunneling current, we are able to fabricate patterns that are different in size but in which the dwell time of the tip per unit area is constant; that is, the Coulomb dose per unit area is constant for the patterns. Under these conditions we expect the depth and RRF of the different size patterns to be approximately the same even though their dimensions in the plane of the substrate vary.

Figure 6 contains STM images of three patterns nominally 50, 100, and 200 nm square, fabricated by depositing a constant Coulomb dose into different-sized patterns using the conditions noted in Table 4. As shown in Table 4, the depth, rms roughness, and RRF for all three patterns are independent of the feature size. Consistent with our proposed electrochemical patterning mechanism, these results show that the Coulomb dose is an important factor in patterning at biases between ∼+2.3 and 3.0 V.

Conclusion

STM-induced lithographic fabrication of patterns in *n*-alkanethiol-coated surfaces is a complex process controlled by numerous parameters, including the relative humidity, tip−substrate bias, and total Coulomb dose. These parameters can be controlled by varying experimental conditions such as the scan rate, tunneling current, and number of patterning scans to obtain desired pattern dimensions. On the basis of our previous work, which showed that patterning was critically dependent on the

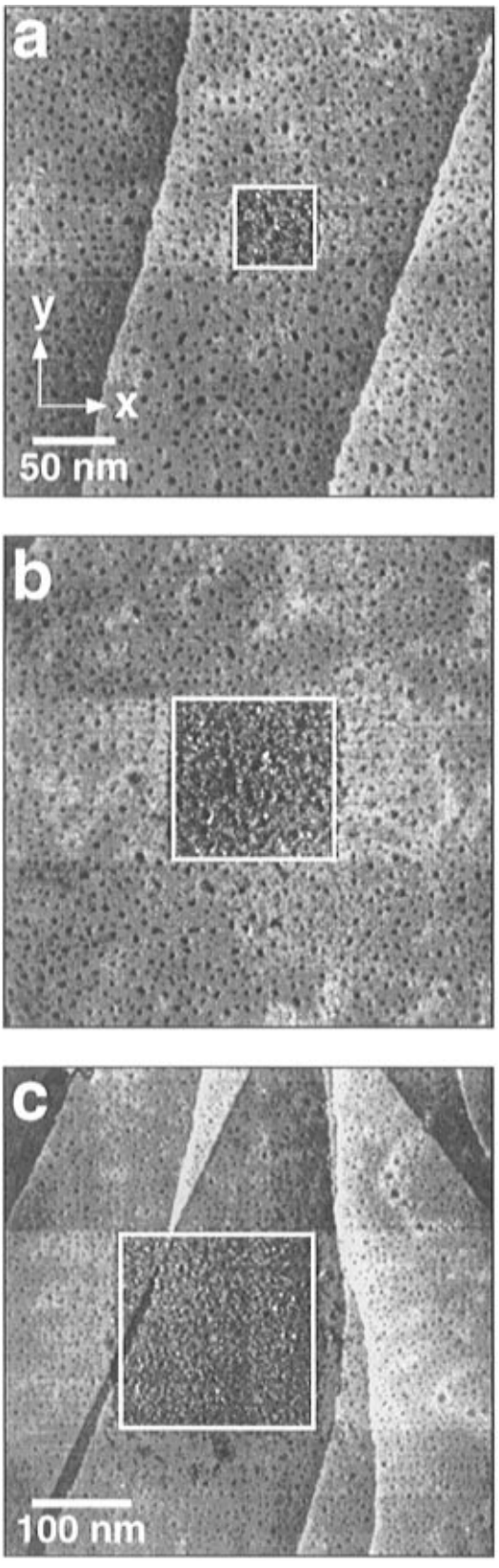

Figure 6. STM images of (a) 50 nm × 50 nm, (b) 100 nm × 100 nm, and (c) 200 × 200 nm patterns fabricated by applying a constant Coulomb dose per unit area. Tunneling current = 150 pA and gap bias = 3.0 V. The gray scale is 2 nm. Table 4 lists the patterning conditions and some physical characteristics of the resulting patterns.

Table 4. Summary of the Conditions Used To Fabricate the Features in Figure 6 Using Conditions That Establish Constant Coulomb Dose per Unit Area and the Physical Characteristics of the Resulting Features[a]

	patterning conditions			pattern characteristics				
figure	nominal pattern size (nm)	patterning scan rate (Hz)	patterning resolution (pixels)	*x*-width (nm)	*y*-width (nm)	*z*-depth[b] (nm)	RMS roughness (nm)	RRF[c]
6a	50	40	128	54	52	0.30	0.29	1.3
6b	100	20	256	102	105	0.26	0.29	1.4
6c	200	10	512	207	211	0.28	0.22	1.3

[a] The gap bias was +3.0 V and the tunneling current was 150 pA during fabrication of each pattern. [b] The absolute value of the difference in the *z*-values between the plane of the pattern and the plane of the unpatterned SAM-coated Au(111) terrace. [c] The RRF is the rms roughness of the nominal dimensions of the primary pattern divided by the rms roughness of the surrounding unpatterned terrace. See the Experimental Section for details.

humidity and gap bias,[1] and the experiments discussed here, which describe general characteristics of patterns and show that patterning is current dependent, we propose a mechanism in which Faradaic electrochemistry is principally responsible for SAM removal. To identify the specific electrochemical reaction(s) occurring during lithography, additional experiments will be required.

Although it is unlikely that serial lithographic approaches, such as that described here, will find large-scale applications, it is reasonable to expect they will be useful for preparing one-of-a-kind, nanometer-scale structures and electronic devices. Additionally, STM-induced lithography of *n*-alkanethiol SAMs provides a better understanding of the types of materials and process strategies that will be required for the next generation of nanometer-scale devices. Finally, we gain insight into the physical and chemical properties of the tip region by studying molecular transformations therein.

Acknowledgment. Full support of this research by the Office of Naval Research is gratefully acknowledged. J.K.S. gratefully acknowledges an IBM Manufacturing Research Fellowship and a Joseph W. Richards Summer Fellowship from the Electrochemical Society. We appreciate insightful discussions with Dr. Henry White (University of Utah), Dr. Omourtag Velev, Dr. Roland Allen, and Dr. Michael Weimer (Texas A&M University). The assistance of Francis Zamborini in completing the ECSTM experiments discussed in the supporting material is gratefully acknowledged.

Supporting Information Available: Images, tables, and brief discussions of pattern stability, the effect of increasing the current at biases <+2.3 V, effect of repeatedly scanning within a pattern using SIC, *in-situ* ECSTM of the disordered region after patterning with SPC, and *in-situ* ECSTM of regions within patterns that appear elevated after lithography at biases <∼+2.3 V or in low-humidity environments (10 pages). Ordering information is given on any current masthead page.

LA960369V